Proceedings of the 10th World Congress on Momentum, Heat and Mass Transfer (MHMT 2025)
Barcelona, Spain - April, 2025
Paper No. ICMFHT 139
DOI: 10.11159/icmfht25.139

Numerical Evaluation of Heat Transfer Enhancement through Film Cooling in Cratered Shaped Inclined Holes

Abhishek Verma[1], Deepak Kumar[1], Debi Prasad Mishra[1,2]
[1]Indian Institute of Technology,
Kanpur, India
abhishv@iitk.ac.in; deepakkr@iitk.ac.in
[2]National Institute of Technical Teachers' Training and Research
Kolkata, India
mishra@iitk.ac.in

Abstract **-** The study investigates the film cooling performance of cratered injection holes, a scenario often encountered when thermal barrier coating layers are applied to turbine blades. These cratered holes result from masking the hole area during the application of thermal barrier coatings, leaving the hole surrounded by a thermal barrier coating layer. Compared to standard cylindrical holes, the film performance and behavior are expected to vary for cratered holes. Detailed measurements of film cooling effectiveness and film vorticity are obtained simultaneously using a numerical study. The k-ε turbulence model with standard wall function is used for the three-dimensional flow domain calculations. The study is conducted at a constant mainstream Reynolds number based on free-stream velocity and film hole diameter, with varying blowing ratios. The results indicate a slight enhancement in film cooling effectiveness due to cratering of holes. Specifically, this study investigates the film cooling effectiveness of cylindrical and off-centered forward cratered (OCFC) injection holes across three blowing ratios (BRs) of 0.6, 1.0, and 1.4, using air as the coolant with a density ratio of 1.14. The results demonstrate that cratered holes consistently outperform cylindrical holes in terms of area-averaged cooling effectiveness. The most significant improvement is observed at BR = 1.0, where cratered holes achieve a 48% enhancement.

Keywords**:** cratered holes, film cooling, effectiveness, vorticity, cylindrical shape, gas turbine

1. Introduction

Gas turbine blades rely on effective cooling methods to prolong their lifespan and reduce maintenance costs. In addition to turbulated cooling [1–3], modern blades utilize film cooling to shield their outer surfaces from high-temperature gases. As turbine inlet temperatures rise, there is a growing need for more efficient cooling methods to keep engines operating below failure conditions. For lower temperature environments, simple cylindrical holes, angled along the flow direction, is sufficient. As discrete holes drilled into the blade's exterior allow internal cooling air to form a protective film on the surface [4–6]. TBCs (thermal barrier coating) are now commonly used in gas turbine, thermal reactor and power plant applications. There are thin layers applied to metal surfaces after the hole areas have been masked off. Masks can create holes embedded in trenches or craters, affecting film cooling characteristics. Nowadays, in some high-temperature operations outside of aviation, turbine blades are coated with high-grade ceramic TBC coatings to further shield them from hot gases [7-9]. Cratering or trenching may transform mainstream-coolant interaction into a more uniform cooling phenomenon. Although designing a single film cooling hole involves various geometric parameters such as hole exit shape, coolant jet inclination angle, hole aspect ratio, and compound angle, the current work focuses on varying hole exit configurations. Goldstein et al. [10] first studied the impact of hole shape on film cooling performance in 1974, using a laterally diffused fan-shaped hole with a 10° diffusion angle. The widened jet exit decelerates the cooling fluid, resulting in higher cooling area coverage and effectiveness. Since then, various hole shapes have been developed, including conical-shaped, fan-shaped with laterally expanded, laid-back-shaped and console holes [11–13]. Shaped holes maintain higher film cooling effectiveness at blowing ratios (BR > 0.5), where coolant jets from cylindrical injection fail. The round film cooling geometries with triangular tabs have also been studied [11]. An upstream triangular notch generates an anti-kidney-pair vortex on top of the cooling jet, reducing penetration into the hot mainstream gas, leading to an almost 300% increase in local adiabatic effectiveness across various blowing ratios (0.5 < BR < 2).

Recently, round holes embedded in crater depressions [14] and trenches [15] have shown substantial benefits in film cooling effectiveness. This approach provides a secondary expansion zone at the exit of the delivery tube, potentially

reducing the coolant jet's momentum flux and increasing its spread before emerging onto the component surface, offering an effective method to enhance cooling. Despite the significant improvements provided by laterally defused holes over cylindrical round holes [9,16,17], there is ongoing interest in exploring other modified hole shapes or injection exit configurations for greater lateral coverage and higher thermal capacity.

This study examines cratered cooling hole geometries and their impact on film cooling heat transfer and effectiveness over flat surfaces. While previous research has shown that cratered film holes improve effectiveness compared to round holes, especially at higher blowing ratios, the effect of cratered geometry on vortex interactions has not been thoroughly explored. Other studies have indicated higher effectiveness for holes embedded in trenches, and recent research suggests that the exit area and shape of cratered holes significantly affect film cooling performance. Computational fluid dynamics studies reveal that cratered holes generate weaker counter-rotating vortex pairs than cylindrical holes, leading to stronger film dissipation downstream, with turbulence intensity similar to baseline cases. This study investigates the impact of blowing ratio, injection geometry, and vorticity on film effectiveness, with varying velocity gradients. A three-dimensional RANS approach is employed using the k-ε turbulence model for BRs of 0.6, 1.0, and 1.4. The injection geometry and vorticity from the jet in cross flow are optimized to enhance heat transfer between the fluids. Previous analyses of cylindrical injection holes have not adequately considered the crucial effect of cratered holes on cooling effectiveness, particularly regarding changes in injection outlet velocity ratios. This numerical analysis uses a three-dimensional domain to compare cylindrical holes and off-centered forward cratered (OCFC) hole, examining how vortex interactions and blowing ratios impact the coolant film across a flat surface.

2. Computational Domain Setup and Specifications

To investigate the three-dimensional geometric effects, vortex formation, temperature distribution, and associated fluid flow impacts on air-film cooling, this study examines two cases: a cylindrical hole and a crater attached to a cylindrical metering tube. As shown in Fig. 1 and 2, the crater depth is 0.75 mm, attached to a circular tube. The rectangular flow domain is divided into three zones: the main flow duct, injection tubes, and a settling chamber. The computational domain dimensions are 46D in length and 22D in height, with the crater located 26D from the mainstream entrance (see Fig. 1). The streamwise injection angle (α) is set at 35°, identified as the optimal value [14, 15]. The coolant outlet from the crater provides a wider spread of cooling air, enhancing cooling effectiveness by reducing jet momentum and increasing lateral coverage on the surface.

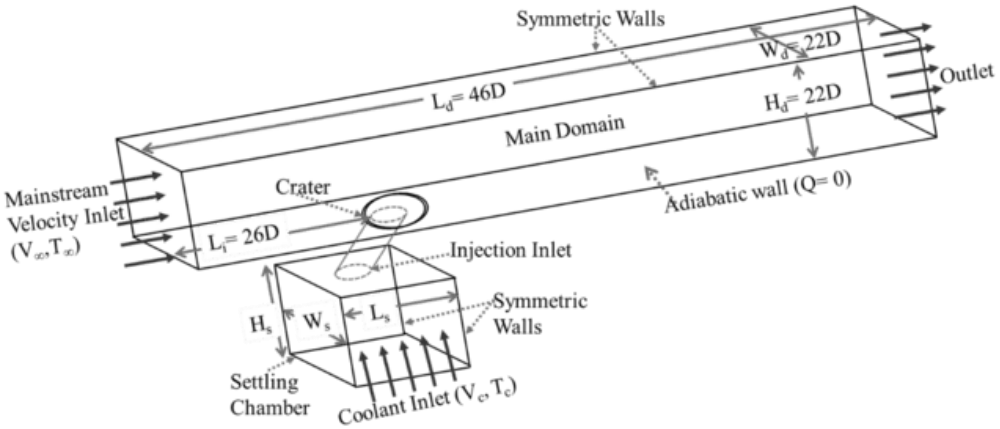

Figure 1. Schematic diagram of the three-dimensional computational domain and cooling hole configuration

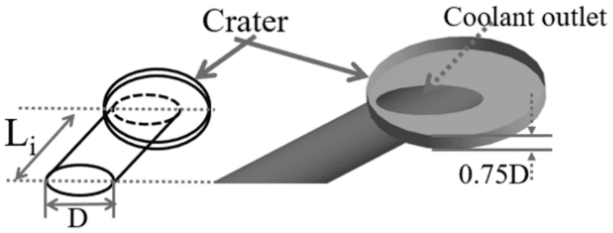

Figure 2. Schematic and three-dimensional computer-aided design of the off-centered forward cratered (OCFC) hole for coolant gas attached with cylindrical metering tube configuration

The length of the metering tube (L_i) is 0.75D. Note that the length of the coolant hole and the preceding settling chamber can influence the numerical results of film cooling. The effect of the settling chamber is not considered in this research and is beyond the scope of this study. Both holes have an entry diameter (D) of 6.35 mm. The length and width of the settling chamber are maintained at 14D, as shown in Fig. 1.

3. Grid Construction

To facilitate numerical calculations, a hexa-structured multi-block computational grid was generated using the ICEM-CFD grid generator, comprising over 7.9 million cells for the cylindrical case (Fig. 3) and a comparable number for the cratered injection case (Fig. 4). Figure 3(a) delineates the computational domain for the cylindrical injection, while Fig. 4(a) shows the domain for the cratered shape case examined and compared in this study. The adoption of a multi-block structured meshing technique ensures precise simulations. As depicted in Figs. 3(a) and 4(a), the grid density is significantly increased near the flat adiabatic surface and the inlet of the film cooling injection through the use of inflation layers, thereby enhancing the accuracy of the film cooling results and accurately capturing the mixing of the two gases. To cool the flat surface with a coolant film, single cylindrical and cratered holes are employed. Each hole has an inlet diameter (D) of 6.35 mm, with the injection tube length being three times the hole diameter (3D) [19,20]. Figures 3(b)-(c) and 4(b) illustrate the injection meshing concentrated near the hole exit.

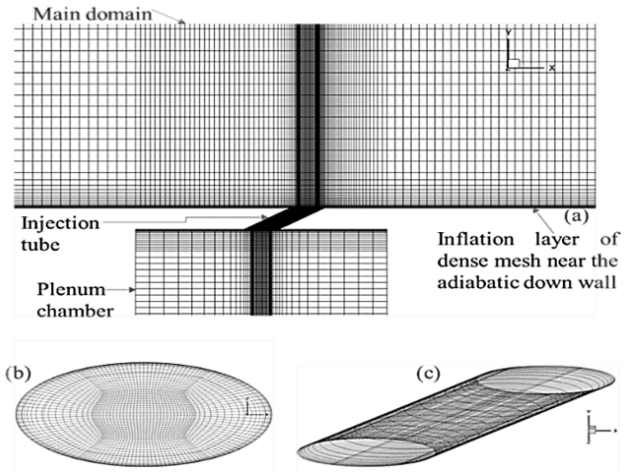

Fig. 3: (a). Meshing of computational domain with injection and plenum section for cylindrical hole case, (b). Meshing of the cylindrical injection outlet, (c). Isometric view of meshing for injection tube.

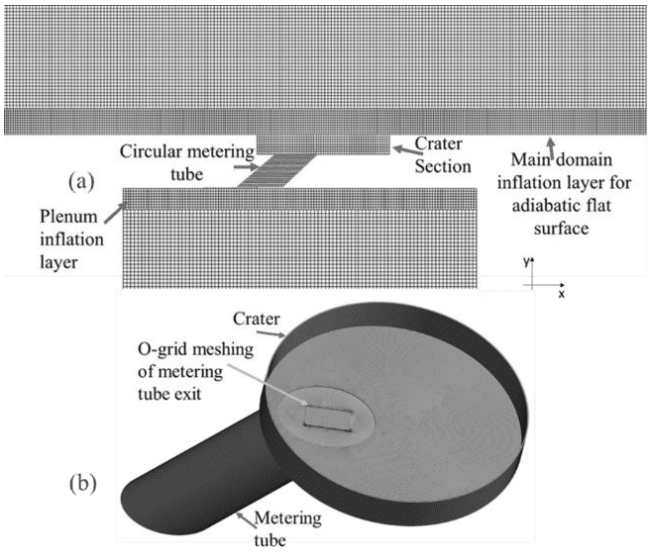

Fig. 4: (a). Meshing of computational domain with injection and plenum section for crater injection case, (b). Meshing of the crater outlet and Isometric view of meshing for injection tube.

The o-grid procedure is applied to the metering section to control the skewness of the individual mesh cells, which is crucial for obtaining accurate and meaningful calculation results. This advanced meshing technique ensures that the mesh quality is maintained throughout the computational domain, particularly in regions where precise flow characteristics are essential. By minimizing cell skewness, the o-grid method enhances the resolution and accuracy of the simulation, allowing for a more detailed and reliable examination of near-hole variations in film performance. This meshing strategy is especially important for capturing intricate details of the flow field, such as velocity gradient and vortex formation. Accurate mesh generation in the vicinity of the injection holes enables the simulation to precisely model the interactions between the coolant jets and the mainstream flow. This results in a more comprehensive understanding of the cooling effectiveness and the behavior of the vortices generated by the jet in crossflow.

4. Numerical Procedure and Turbulence Model

The study utilizes the commercial software package ANSYS-fluent. Based on the three-dimensional, steady-state, incompressible RANS equations, including the energy equation [18], a mathematical model was developed. The Standard k-ε turbulence model was utilized to enhance predictions of fluid mixing and coolant dispersal patterns. The reason behind the selection of k-ε turbulence model is that it also can perform more effectively for several flow types like boundary layer flows in environments with significant temperature gradients. Additionally, it can identify critical phenomena such as flow recirculation. The k-ε turbulence model plays a significant role in the simulation of film cooling scenarios within gas turbine engines, where it is widely used to predict film temperature distribution and momentum transfer characteristics around component surface. One of the main advantages of utilizing the k-ε turbulence model in cooling applications is its ability to effectively capture the effects of turbulence that influence heat transfer characteristics, allowing for accurate predictions of coolant film behavior. Numerous studies [3,4,6] have demonstrated its effectiveness, revealing that the model accurately predicts cooling effectiveness under various operational conditions, including changes in blowing ratio and turbulence intensity.

4.1 Mathematical Framework

To analyze fluid flows, the transport equations for incompressible mass conservation, momentum, and energy must be evaluated. For turbulent flows, additional transport equations are required, and turbulence models are applied to account for these equations and include dissipation effects. Assuming constant fluid properties is a valid simplification based on empirical evidence. The convergence criteria for the continuity equation residuals were set at 10^{-6}, while the residuals for velocity and energy components were consistently less than 10^{-8} and less than 10^{-4} for k and ϵ at convergence. The second-order upwind discretization method was employed to discretize the momentum, energy, and pressure variables.

Continuity and Momentum Equations. The equations of mass and momentum conservation are fundamental to understanding fluid dynamics, and their resolution is essential for analyzing all types of flows. However, turbulent flow introduces complexities that necessitate the solution of additional transport equations. This section explores the conservation equations used to address turbulent flows in a non-accelerating reference frame.

$$\frac{\partial}{\partial x_i}(\rho u_i) = 0 \tag{1}$$

$$\frac{\partial}{\partial x_j}\left(\rho u_i u_j\right) = -\frac{\partial p}{\partial x_j} + \frac{\partial}{\partial x_j}\left[\mu\left(\frac{\partial u_i}{\partial x_j} + \frac{\partial u_j}{\partial x_i} - \frac{2}{3}\delta_{ij}\frac{\partial u_l}{\partial x_l}\right)\right] + \frac{\partial}{\partial x_j}\left(-\rho\overline{u_i' u_j'}\right) \tag{2}$$

Energy Equations. In the present analysis, where heat transfer occurs between two distinct gas streams, it is imperative to consider the conservation of energy as well.

$$\frac{\partial}{\partial x_i}\left(\rho u_i c_p T\right) = \frac{\partial}{\partial x_j}\left[\left(\lambda + \frac{c_p \mu_t}{Pr_t}\right)\frac{\partial T}{\partial x_i}\right] \tag{3}$$

Realizable k-ε Model. The underlying transport equations provide the turbulence kinetic energy (k), and its rate of dissipation (ε):

$$\frac{\partial}{\partial x_j}(\rho k u_i) = \frac{\partial}{\partial x_j}\left[\mu + \left(\frac{\mu_t}{\sigma_k}\right)\frac{\partial k}{\partial x_j}\right] + G_k + G_b + \rho\varepsilon - Y_M \tag{4}$$

$$\frac{\partial}{\partial x_j}(\rho \varepsilon u_i) = \frac{\partial}{\partial x_j}\left[\mu + \left(\frac{\mu_t}{\sigma_\varepsilon}\right)\frac{\partial \varepsilon}{\partial x_j}\right] + \left(C_{1\varepsilon}\frac{\varepsilon}{k}C_{3\varepsilon}G_b\right) + \rho C_1 S_\varepsilon - \rho C_2 \frac{\varepsilon^2}{k + \sqrt{\varepsilon\nu}} \tag{5}$$

In the above equations, G_k denotes the turbulence kinetic energy production by the mean velocity gradients. $C_{1\varepsilon}$ and C_2 are constants. The turbulent Prandtl numbers are denoted by σ_k and σ_ε.

$$G_k = \overline{\left(-\rho u_i' u_j'\right)}\frac{\partial u_i}{\partial x_j} \tag{7}$$

Equation (8) is employed to determine the local values of film cooling effectiveness on the surface. In this analysis, it is crucial to note that the plate is adiabatic (Q=0), indicating no heat transfer. As depicted in Fig. 1, the temperature of the local film, distributed across the wall, corresponds to the adiabatic wall temperature (T_{aw}). Adiabatic film effectiveness (η) is normalized by the temperature difference between the mainstream gas (T_∞) and the coolant gas (T_c). The local values of film cooling effectiveness over the surface are computed using Eq. (8),

which quantifies the efficiency of the coolant film in protecting the surface. This is achieved by comparing the local wall temperature (T_{aw}) to the temperatures of the mainstream (T_∞) and coolant gases (T_c). This normalization allows for a standardized comparison of film cooling performance under different injection geometric conditions.

$$\eta = \frac{T_{aw} - T_\infty}{T_c - T_\infty} \tag{8}$$

$$BR = \frac{V_c \rho_c}{V_\infty \rho_\infty} \tag{9}$$

where V_c and ρ_c represent the coolant velocity and density, respectively, at the injection inlet averaged over the entire span. Conversely, V_∞ and ρ_∞ denote the mainstream gas velocity and density, respectively, at the main duct inlet averaged over the surface.

5. Boundary Conditions

Figure 1 illustrates the components and boundary conditions of the computational domain, which includes velocity inlets, an adiabatic down wall, a pressure outlet, symmetric surfaces, and other domain walls, each with specific boundary conditions. To ensure consistent reference values, a high-temperature gas velocity of 20 m/s is defined at the entry of the main domain [19,20]. Table 1 provides a comprehensive overview of all boundary conditions associated with their respective zones.

Table 1. Computational domain boundary conditions

Region	Boundary Condition	Value
Main-domain hot gas inlet	Velocity Inlet	V_∞=19.8 m/s, T_∞=320K
Coolant gas inlet	Velocity Inlet	BR=0.6 to 1.4, T_c=280K
Main-domain outlet	Pressure Outlet	1 atm
Side walls of main domain	Symmetric	-
Side walls of the plenum	Symmetric	-
All other walls	No-Slip Walls	-

6. GRID INDEPENDENCE TEST

A study on grid independence was performed to determine the optimal mesh size for both of the injection cases. At a BR of 0.6, five various grid sizes were evaluated. The simulation employs a pressure-based solver, and the SIMPLE algorithm is used to couple pressure and velocity. The grid independence test illustrated in the Fig. 5 compares the temperature profiles along the normalized distance X/D for five different grid sizes in a cylindrical and crater case.

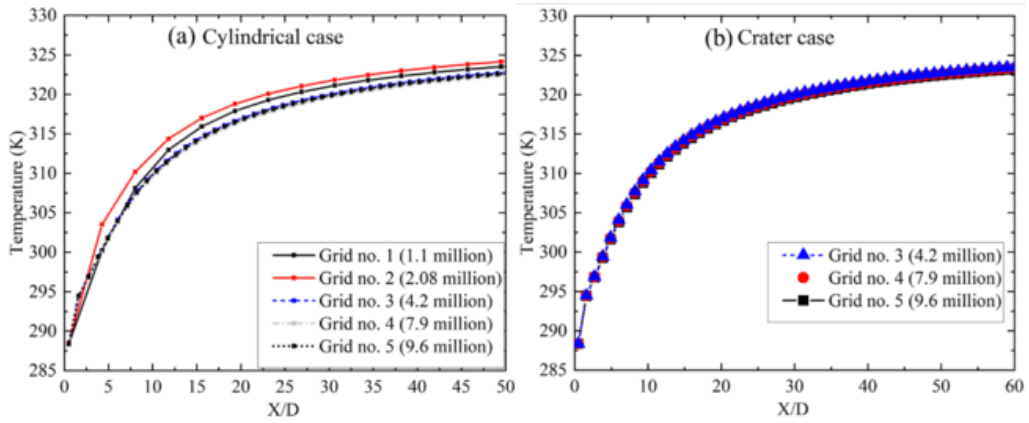

Fig. **5.** Grid independence test results for (a). cylindrical and (b). crater case

The grids range from 1.1 million to 9.6 million cells. The temperature profiles converge as the grid size increases, with minimal differences observed between grid no. 3 (4.2 million cells), grid no. 4 (7.9 million cells), and grid no. 5 (9.6 million cells) in both of the injection cases. This indicates that these grids are approaching grid independence, ensuring that further refinement does not significantly affect the results. grid no. 4 is deemed optimal, balancing accuracy and computational efficiency. The upcoming sections that follow present numerical findings based on grid number 4.

7. RESULTS

7.1 Validation of Present simulations

The numerical model has been verified by comparing its results with the operational characteristics previously discussed and the findings of earlier studies on cylindrical injection holes [19]. The current data on centerline film cooling effectiveness were normalized using the coolant temperature from Zhao et al.'s two-phase flow study, where the coolant gas temperature was lowered due to the evaporation of suspended water droplets [19, 20]. By using this existing data, the film effectiveness along the centerline was evaluated at a mass flux ratio of 0.6 to ensure the model's accuracy. Figure 6 shows the agreement between the model's predictions and preliminary experimental findings, although a slight over-prediction is observed. It is important to note that uncertainties in the referenced experiment and limitations of the turbulence model used in the simulation may contribute to the observed discrepancy between the simulated and experimental results. Additionally, the fluid near the injection point, where the coolant first meets the mainstream fluid, can be affected by several other factors such as surface roughness and the sharp edge of the coolant injection. These factors can significantly alter vortex behavior, which may explain the larger difference observed between the experimental and numerical results at X/D = 5, as shown in Fig. 6.

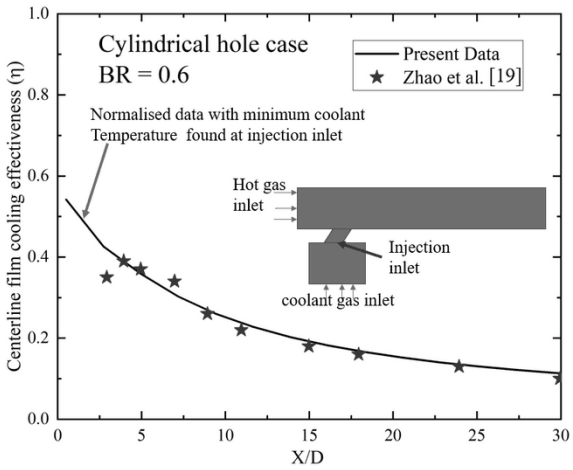

Fig. 6. Validation of present numerical study with previous experimental data [19] for a cylindrical coolant injection hole at BR = 0.6.

7.2 Vorticity Variations with Blowing Ratio

The vorticity, which is a measure of the local rotation in a fluid flow, and the velocity gradient variation are analyzed in this section. The x-component of vorticity, often referred to as ω_x, represents the rotation or spinning of fluid elements around the x-axis. The x-vorticity, as plotted in Fig. 7 for cylindrical injection cases and in Fig. 8 for crater cases, is a crucial parameter in understanding the rotational dynamics of the flow. As the flow in this study is three-dimensional, x-vorticity is significant as it indicates the rotation of fluid elements about the x-axis due to variations in the transverse velocity components. This term is important in film cooling to understand the lateral spread and mixing of the coolant gas at the exit of the injection and over the expanded surface as it moves in the X/D direction. At a BR of 0.6, the cylindrical hole exhibits strong and concentrated regions of vorticity, as illustrated in Fig. 7, indicating significant formation of vortices near the injection hole at a normalized distance of X/D=3. This causes the intense mixing of the coolant air with the hot mainstream, increasing the temperature of the cooling film over the flat surface. Although the BR is low, there is no separation of the film from the surface, which is beneficial. These results for the cylindrical hole are consistent with previous studies [4,15,16] that identified BR = 0.6 as the optimal BR for cylindrical cases.

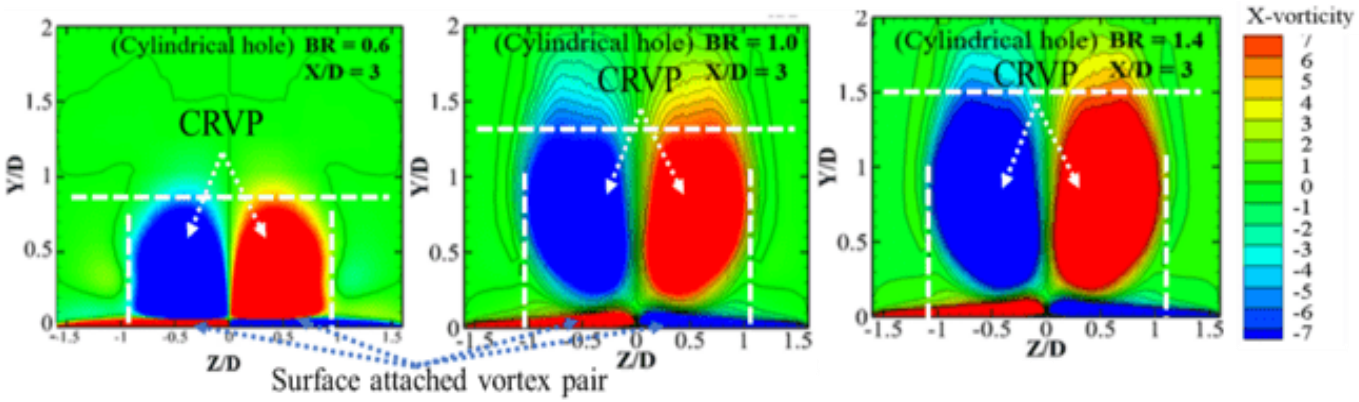

Fig. 7. Lateral variation of turbulent kinetic energy for different blowing ratios (BR = 0.2 to 2.0) at several stream-wise locations (X/D = 0.5, 2.5, & 5.0).

In contrast, the cratered hole exhibits a more diffused vorticity field with broader, less concentrated regions of vorticity as shown in Fig. 8. This indicates vortex formation with a comparatively lower strength than in the cylindrical case. The coolant jet remains closer to the surface, enhancing lateral spread compared to the cylindrical case and reducing jet lift-off, resulting in more uniform cooling coverage. When the BR is increased from 0.6 to 1.0, the contour of x-vorticity for both cylindrical and cratered holes at the same streamwise distance shows consistent trends. The vorticity strength is higher in the cylindrical case, indicating increased mixing of the hot mainstream with the coolant. Due to the increased momentum of the jet, separation starts near the injection point. On the other hand, at BR = 1.0, the cratered hole shows less vorticity strength compared to the cylindrical case. However, with the increase in BR, there is a minimal increase in vorticity in the cratered case. The lateral expansion is more pronounced in the cratered case at BR = 1.0, indicating better coolant spread and coverage. At a higher BR of 1.4, the vorticity continuously intensifies for both injection cases, as shown in Figs. 7 and 8. Higher BRs are unsuitable for the cylindrical case as the jet penetration and mixing of the coolant become more pronounced.

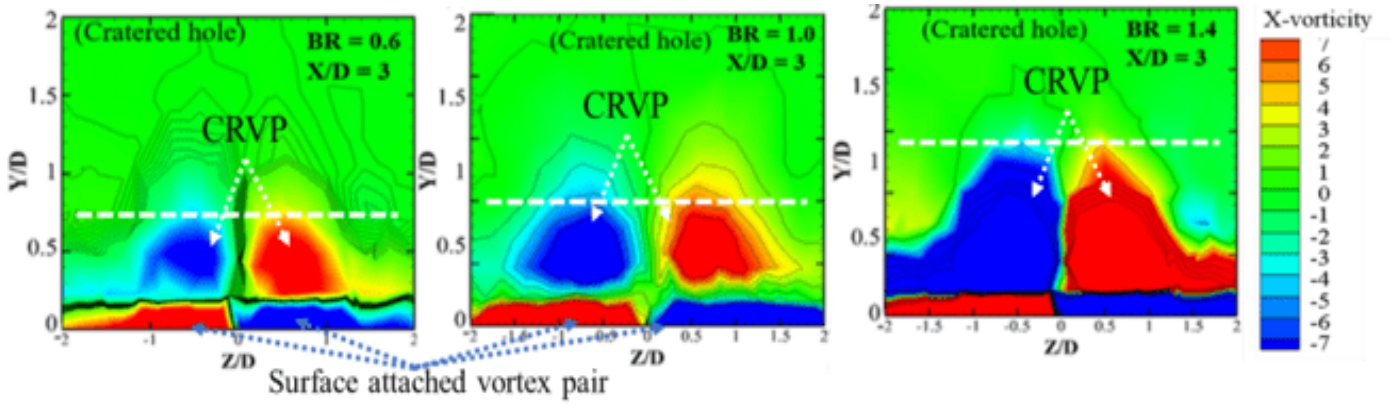

Fig. 8. Lateral variation of turbulent kinetic energy for different blowing ratios (BR = 0.2 to 2.0) at several stream-wise locations (X/D = 0.5, 2.5, & 5.0).

The high momentum of the strongly revolving vortical structures lifts the coolant film, causing it to detach from the surface. This detachment significantly reduces the cooling effectiveness by preventing the coolant from maintaining close contact with the surface. In contrast, while the vorticity also increases for the cratered hole at higher BRs, the coolant jet remains closer to the surface due to the injection's geometric features. There is still considerable lateral spread of the film, though slightly less than at BR = 0.6 and 1.0, and a slight jet lift-off is identified near the injection in this case too. Thus, higher BRs exacerbate the inefficiencies in cylindrical holes but do not severely impact the performance of cratered holes, which continue to provide more effective and uniform cooling coverage. The white dotted lines indicate the maximum expansion of the vorticity along the yz plane. The vertical and lateral expansion of the vortex can be easily compared by observing the white lines in Fig. 7. It has been noticed that the vertical expansion of the vortex is more than the lateral expansion in the cylindrical case, which increases with BR. This means that coolant jets with higher momentum fly away with the mainstream hot gas at BR = 1.4, resulting in a low cooling effect on the surface. On the other hand, vertical expansion is less in the cratered injection hole case, resulting in more sophisticated cooling at higher BRs. These consistent trends reinforce the conclusion that cratered holes provide superior cooling performance by maintaining the coolant jet closer to the surface and achieving more uniform lateral spread, highlighting the superiority of cratered holes over cylindrical holes for film cooling applications.

7.3 Geometric Impact on Effectiveness Distribution

The injection geometric impacts on effectiveness with varying BRs are investigated in this section. Film effectiveness results are presented for three blowing ratios of 0.6, 1.0, and 1.4, with a density ratio of 1.14 (air), and two injection geometries: cylindrical and cratered holes. Figure 9 and 10 illustrates the local film effectiveness distributions for air injection. The cratered holes demonstrate superior performance, with higher effectiveness values and better lateral spread of coolant. The diffused vorticity field in cratered holes as discussed in previous section, enhances lateral spread and maintains the coolant film closer to the surface, resulting in more uniform cooling coverage. At BR = 1.0, cratered holes maintain their superiority with a broader and more uniform effectiveness distribution laterally. At BR = 1.4, while the effectiveness decreases for both configurations, cratered holes still perform better except the region up to X/D = 5, providing more effective coverage than cylindrical holes specially for longer X/D distance.

At BR = 0.6, the peak enhancement of 20% is found at X/D=7 compared to the cylindrical case due to the immediate and effective lateral spread of the coolant. Also, the higher film cooling effectiveness at BR = 0.6 is attributed to the expansion of the coolant jet at the crater of the injection, which causes most of the coolant fluid to remain attached for a longer X/D distance. The percentage enhancement is particularly significant at BR = 1.0, reaching approximately 48%. This enhancement is due to the controlled and diffused vorticity field produced by cratered holes, which reduces jet lift-off and ensures better cooling coverage. In contrast, the presence of a vortex pair that causes further lateral dispersion of the film in the cratered hole case can be attributed to increased effectiveness near the injection hole (X/D<5) for blowing ratios of 0.6 and 1.0.

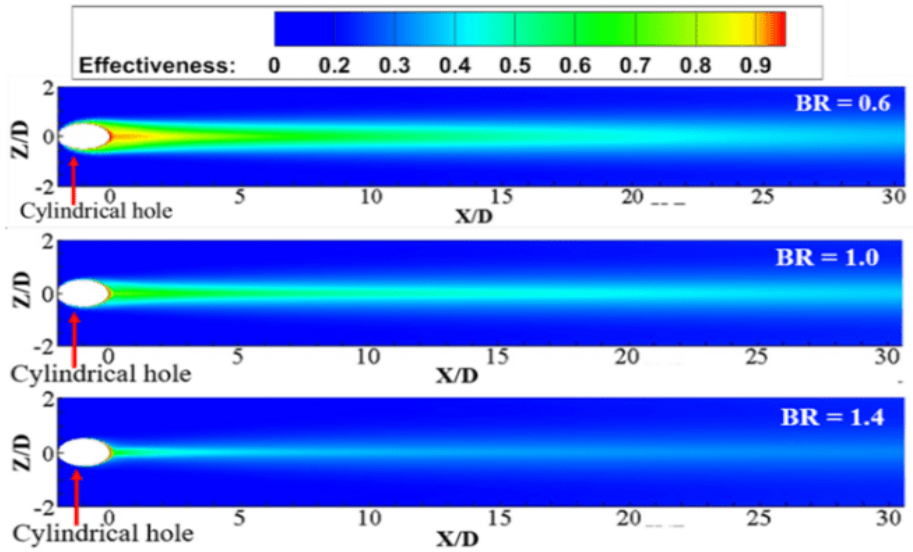

Figure 9. Lateral distribution of effectiveness for cylindrical hole injection at different BRs along X/D

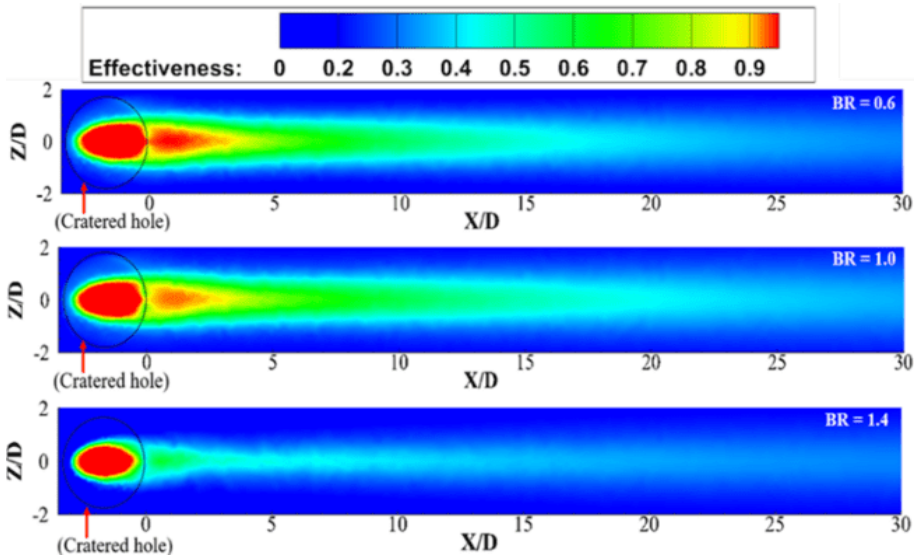

Figure 10. Lateral distribution of effectiveness for cratered injection hole at BR = 0.6, 1.0, and 1.4 along X/D

8. Conclusions

Film cooling plays a vital role in managing heat transfer and temperature distribution on aircraft components, such as turbine blades and combustor liners. This numerical study investigates film cooling effectiveness for three blowing ratios of 0.6, 1.0, and 1.4 using air (density ratio of 1.14) as the coolant, focusing on cylindrical and cratered hole geometries. Based on the findings, it can be concluded that injection geometry plays a crucial role in determining the film cooling performance of the system. The distribution of effectiveness and vorticity determines the nature of coolant jet spreading over the surface and the effectiveness of film cooling.

- The cratered holes consistently outperform cylindrical holes across most conditions, except at BR = 1.4 near the injection site. the Cratered holes at the same BR show higher effectiveness due to a diffused vorticity field that promotes immediate and effective lateral coolant spread, reducing jet lift-off and ensuring better cooling coverage.
- The high momentum due higher BR coolant fluid in cratered holes encounters the edge effect after expansion, causing film separation and reduced near-hole effectiveness.
- Cylindrical holes, on the other hand, show reduced effectiveness at higher BRs due to increased vorticity and film separation.

In conclusion, cratered holes demonstrate superior performance by maintaining better lateral and vertical spread, reducing jet lift-off, and ensuring effective film cooling coverage, underscoring their advantages over cylindrical holes. The findings of this study have important implications for the design and optimization of film cooling systems. By considering the vorticity distribution and injection geometry, it can be possible to improve film cooling effectiveness and surface protection. Further research in this area could lead to significant improvements in the efficiency and performance of film cooling systems, with potential applications in a wide range of industries.

NOMENCLATURE

BR	Blowing ratio
CRVP	Counter-rotating vortex pair
MR	Momentum flux ratio

X/D	Streamwise dimensionless distance
Z/D	Lateral dimensionless distance
G_b	The production of turbulence kinetic energy due to buoyancy
Y_M	Contribution of the fluctuating dilatation
L_i	Length Between Domain Inlet to Leading Edge of The Hole
H_d	Main duct height
L_d	Main duct length
L_s	Plenum (or settling chamber) Length
H_s	Plenum (or settling chamber) Height
W_d	Main Duct width
W_s	Settling chamber width
DNS	Direct numerical simulation
H	Centerline film cooling effectiveness
ξ	Area averaged film cooling effectiveness

Greek

α	Forward injection angle

Subscript

aw	Adiabatic wall
c	Coolant
∞	Mainstream

References

[1] L. Wright, A. Gohardani, Effect of Coolant Ejection in Rectangular and Trapezoidal Trailing-Edge Cooling Passages, J. Thermophys. Heat Transf. 23 (2009) 316–326. https://doi.org/10.2514/1.38426.

[2] X. Li, T. Wang, Simulation of Film Cooling Enhancement with Mist Injection, J. Heat Transfer. 128 (2006) 509–519. https://doi.org/10.1115/1.2171695.

[3] T.S. Dhanasekaran, T. Wang, Computational Analysis of Mist/Air Cooling in a Two-Pass Rectangular Rotating Channel with 45-Deg Angled Rib Turbulators, Int. J. Heat Mass Transf. 61 (2013) 554–564. https://doi.org/10.1016/j.ijheatmasstransfer.2013.02.006.

[4] A. Brown, C.L. Saluja, Film Cooling from a Single Hole and a Row of Holes of Variable Pitch to Diameter Ratio, Int. J. Heat Mass Transf. 22 (1979) 525–534. https://doi.org/10.1016/0017-9310(79)90056-5.

[5] M. Gritsch, A. Schulz, S. Wittig, Discharge Coefficient Measurements of Film-Cooling Holes with Expanded Exits, J. Turbomach. 120 (2011) 557. https://doi.org/10.1115/1.2841753.

[6] S. Wittig, A. Schulz, Transonic Film Cooling Investigations: Effects of Hole Shapes and Orientations, Am. Soc. Mech. Eng. (1996).

[7] K. Kadotani, R.J. Goldstein, Effect of Mainstream Variables on Jets Issuing from a Row of Inclined Round Holes, J. Eng. Power. 101 (1979) 298. https://doi.org/10.1115/1.3446486.

[8] Y. Lu, A. Dhungel, S. V Ekkad, R.S. Bunker, Effect of Trench Width and Depth on Film Cooling from Cylindrical Holes Embedded in Trenches, Mech. Eng. (2007) 1–11.

[9] X.-M. Tan, J.-Z. Zhang, Q.-Z. Cai, Effects of Pin-Fin Shapes on Mesh-Fed Slot Film Cooling for a Flat-Plate Model, J. Therm. Sci. Eng. Appl. 11 (2018) 031002. https://doi.org/10.1115/1.4041882.

[10] R.J. Goldstein, E.R.G. Eckert, F. Burggraf, Effects of Hole Geometry and Density on Three-Dimensional Film Cooling, Int. J. Heat Mass Transf. 17 (1974) 595–607. https://doi.org/10.1016/0017-9310(74)90007-6.

[11] L. Zhong, C. Zhou, Z. Sun, S. Chen, Heat Transfer Mechanisms of Inclined Jets in Cross Flow with Different Holes, Int. J. Heat Mass Transf. 131 (2019) 664–674. https://doi.org/10.1016/j.ijheatmasstransfer.2018.11.095.

[12] R.S. Bunker, A Review of Shaped Hole Turbine Film-Cooling Technology, J. Heat Transfer. 127 (2005) 441–453. https://doi.org/10.1115/1.1860562.
[13] J. Zhou Zhang, X. Dan Zhu, Y. Huang, C. Hua Wang, Investigation on Film Cooling Performance From a Row of Round-To-Slot Holes on Flat Plate, Int. J. Therm. Sci. 118 (2017) 207–225. https://doi.org/10.1016/j.ijthermalsci.2017.04.029.
[14] Y. Lu, A. Dhungel, S. V. Ekkad, R.S. Bunker, Film Cooling Measurements for Cratered Cylindrical Inclined Holes, J. Turbomach. 131 (2008) 011005. https://doi.org/10.1115/1.2950055.
[15] P. Kalghatgi, S. Acharya, Improved Film Cooling Effectiveness with a Round Film Cooling Hole Embedded in a Contoured Crater, J. Turbomach. 137 (2015) 101006. https://doi.org/10.1115/1.4030395.
[16] J.H. Kim, K.Y. Kim, Film-Cooling Performance of Converged-Inlet Hole Shapes, Int. J. Therm. Sci. 124 (2018) 196–211. https://doi.org/10.1016/j.ijthermalsci.2017.10.014.
[17] D. Zheng, X. Wang, Q. Yuan, Numerical Investigation on The Effect of Upstream Ramps on Film Cooling Performance with Backward Injection, Microsyst. Technol. 8 (2019). https://doi.org/10.1007/s00542-019-04303-8.
[18] Ansys Fluent Theory Guide, Ansys Inc., Usa. 15317 (2013) 724–746.
[19] L. Zhao, T. Wang, An Experimental Study of Mist/ Air Film Cooling on a Flat Plate with Application to Gas Turbine Airfoils-Part I: Heat Transfer, J. Turbomach. 136 (2014) 1–9. https://doi.org/10.1115/1.4025736.
[20] L. Zhao, T. Wang, An Experimental Study of Mist/Air Film Cooling on a Flat Plate with Application to Gas Turbine Airfoils-Part II: Two-Phase Flow Measurements and Droplet Dynamics, J. Turbomach. 136 (2014) 1–9. https://doi.org/10.1115/1.4025738.